JOURNAL OF COMPUTATIONAL PHYSICS 66, 274–293 (1986)

Computation of Visco-resistive MHD Instabilities

R. J. HOSKING

University of Waikato, Hamilton, New Zealand

AND

J. TENDYS

Australian Atomic Energy Commission,
Lucas Heights, New South Wales 2232, Australia

Received January 8, 1985; revised May 28, 1985

DEDICATED TO THE MEMORY OF RAYMOND C. GRIMM

Resistive instabilities may be controlled by wall stabilisation or magneto-viscous damping. From a mathematical model based on MHD equations involving resistivity and parallel ion viscosity, a special purpose computer code has been developed to trace the disturbances of cylindrical equilibria surrounded by conducting walls. Another code, using general purpose collocation software to exploit robust time integrators via the numerical method of lines, may be extended to more sophisticated models. Magneto-viscous reduction of resistive growth rates, due to parallel ion viscosity and independent of conducting wall stabilisation, is most pronounced for smaller axial wavelengths and higher plasma temperatures.

1. INTRODUCTION

Plasma instabilities remain a major obstacle for the magnetic confinement approach to a thermonuclear reactor, and large-scale magneto-hydrodynamic (MHD) modes in particular can be most destructive. Tokamak configurations, with toroidal magnetic flux surfaces created by large applied longitudinal fields and limited longitudinal current, have been investigated extensively. There are also alternative diffuse pinch schemes that deserve more attention. The "reverse-field-pinch" can be *ideal* MHD stable at values of beta, the plasma pressure to magnetic pressure ratio, almost ten times the few percent typical of tokamaks (Robinson [1], Bodin and Newton [2]). The related compact spheromak also relies less on expensive external applied magnetic fields than do tokamaks or stellarators (Rosenbluth and Bussac [3]).

Disturbances occur in the experimental devices, however, even if their magnetic field configurations are stable according to ideal MHD theory. These residual dis-

0021-9991/86 $3.00

turbances have been attributed to finite plasma conductivity (nonzero *resistivity*), which permits access to lower potential energy states that are topologically inaccessible in ideal theory (Furth, Killeen, and Rosenbluth [4]). *Tearing* (*resistive kink* or *current-driven*) instabilities arise in current carrying plasma, and *resistive interchange* (*pressure-driven*) instabilities occur despite magnetic field shear, to further limit the plasma beta. (In toroidal geometry, pressure-driven instabilities found in regions of unfavourable magnetic field curvature are called *ballooning* modes.) These tearing or resistive interchange instabilities can produce large-scale plasma displacements that proceed much faster than classical resistive diffusion. A third type of resistive instability known as *rippling*, which may occur near the plasma boundary, shall not be considered in this paper.

Theoretically, there are ways to avoid or control resistive instabilities. For example, tearing may be avoided in tokamaks by a rather more stringent limit on the longitudinal plasma current, corresponding to a "safety factor" $q(r) = rB_{oz}/RB_{o\theta}$ everywhere greater than about 3 (where r is the minor radius and R the major radius of the torus, B_{oz} is the applied longitudinal or "toroidal" magnetic field, and $B_{o\theta}$ is the azimuthal or "poloidal" magnetic field generated by the plasma current). The high current, high magnetic field shear reverse-field-pinch devices typically have $q(r)$ values much less than 1, but tearing nevertheless may be controlled when there is a conducting wall close enough to the plasma (Robinson [5]). The inclusion of ion magneto-viscosity may also stabilise both tearing and resistive interchange modes in cylindrical geometry; parallel viscosity terms dependent on magnetic field curvature are important (Hosking [6], Hosking and Robinson [7]). Both wall and magneto-viscous stabilisation may be studied by computer codes, as outlined in this paper.

Computer codes are now widely used to simulate the evolution of magnetic field configurations. The growing complexity of stability analysis, which is compounded as the plasma model is extended to include nonideal effects in realistic geometries, has motivated our interest in developing the two codes briefly described in this paper. The first is a traditional special purpose routine to trace the linear departure from cylindrical equilibria (viz. VISCODE), as defined by MHD equations incorporating resistivity and parallel ion viscosity (cf. Dibiase and Killeen [8]). A second code (PDECODE), based on general purpose collocation software to exploit available robust ordinary differential equation integrators via the numerical method of lines, more readily allows extension to other nonideal processes. Our experience in running these codes on quite modest computers (viz. PDP DEC–10 and VAX) leads us to expect such extensions to be quite feasible as available computer power increases.

The visco-resistive model summarised in Section 2 can in principle describe various magneto-plasma regimes; but we have chosen to adopt classical collisional transport coefficients, for the preliminary study of reverse-field-pinch configurations described in this paper. The equilibrium and perturbation equations are summarised in Section 3, and a qualitative analysis of anticipated viscous stabilisation is given in Section 4. The cylindrical equilibria studied appear in Section 5, followed

by a brief discussion of the chosen boundary and initial conditions for the study. The essential six scalar equations for the perturbation fields are summarised in Section 6, and the plasma parameters we adopted are then listed. VISCODE is briefly described in Section 7, and PDECODE in Section 8. Finally, the results obtained in applying these codes to the model reverse-field-pinch configurations are summarised in Section 9.

2. Mathematical Model

The Eulerian form of the magnetohydrodynamic (MHD) equations used to model the visco-resistive plasma include

$$\frac{\partial \rho}{\partial t} + \nabla \cdot (\rho \mathbf{v}) = 0, \tag{2.1}$$

$$\rho \left(\frac{\partial \mathbf{v}}{\partial t} + \mathbf{v} \cdot \nabla \mathbf{v} \right) + \nabla \cdot \mathbf{p} = \mathbf{j} \times \mathbf{B}, \tag{2.2}$$

$$\mathbf{E} + \mathbf{v} \times \mathbf{B} = \frac{1}{\sigma} \mathbf{j}, \tag{2.3}$$

$$\nabla \times \mathbf{B} = \mu_0 \mathbf{j}, \tag{2.4}$$

$$\nabla \cdot \mathbf{B} = 0, \tag{2.5}$$

$$\nabla \times \mathbf{E} = -\frac{\partial \mathbf{B}}{\partial t}, \tag{2.6}$$

where ρ is the mass density, $\mathbf{v}$ is the fluid velocity, $\mathbf{p}$ is the plasma pressure tensor, $\mathbf{j}$ is the electric current density, $\mathbf{B}$ is the magnetic induction, $\mathbf{E}$ is the electric field, σ is the plasma conductivity, and μ_0 the magnetic permeability.

We augment Eqs. (2.1)–(2.6) by the adiabatic equation of state and plasma constitutive relationship as follows:

$$\frac{1}{p} \frac{dp}{dt} = \frac{\gamma}{\rho} \frac{d\rho}{dt}, \tag{2.7}$$

and for each plasma specie

$$\mathbf{p} = p\mathbf{I} + \mathbf{t}. \tag{2.8}$$

Here γ is the ratio of specific heats ($\gamma = \infty$ is the incompressible limit); and the non-hydrostatic part of the stress tensor $\mathbf{t}$, for a sufficiently strong magnetic field, is the expansion ordered in increasing powers of $(\omega_c \tau)^{-1} \ll 1$ (where ω_c is the cyclotron frequency and τ a collision time):

$$\mathbf{t} = \mathbf{t}_{\parallel} + \mathbf{t}_L + \mathbf{t}_{\perp} + \cdots,$$

where

$$\mathbf{t}_{\parallel} = -3\mu_{\parallel}\mathbf{s}\colon \mathbf{bb}\{\mathbf{bb}\} \qquad \text{parallel component,}$$

$$\mathbf{t}_{L} = -\frac{\mu_{\parallel}}{a}\{\mathbf{s}\times\mathbf{b} + 6\{\mathbf{s}\cdot\mathbf{bb}\}\times\mathbf{b}\} \qquad \text{("collisionless") FLR component,}$$

$$\mathbf{t}_{\perp} = -\frac{\mu_{\parallel}}{2a^2}(\mathbf{s} + 6\{\mathbf{s}\cdot\mathbf{bb}\} - \frac{15}{2}\mathbf{s}\colon \mathbf{bb}\{\mathbf{bb}\}) \qquad \text{perpendicular component,}$$

with $\mu_{\parallel}$ the (parallel) viscosity coefficient, the braces $\{\ \}$ denoting the traceless part of the enclosed dyadic, $\mathbf{s}$ the "deformation tensor," and $\mathbf{b} = \mathbf{B}/|\mathbf{B}|$ the local magnetic field direction (cf. Hosking and Marinoff [9]).

We are primarily interested in the *parallel ion viscosity* for it is the dominant part for high temperature magneto-plasma with approximately equal ion and electron temperatures, and may stabilise the resistive instabilities. (Parameter $a \sim \omega_c\tau \gg 1$ for most plasmas of interest, so the so-called FLR and perpendicular viscosity components are ordered smaller. *Electron viscosity* contributions would enter the generalised Ohm's law (2.3) if included, but are omitted from the equation of motion (2.2) because ion collisions are relatively more important [9].) We anticipate that the parallel viscosity coefficient ($\mu_{\parallel}$) rapidly increases with temperature, as the collisions produce increasing particle momentum exchange along the field lines; see Section 6. For the ions, from the simple form of the deformation tensor

$$\mathbf{s} = \{\nabla\mathbf{v}\} = \tfrac{1}{2}(\nabla\mathbf{v} + \mathbf{v}\overleftarrow{\nabla}) - \tfrac{1}{3}\nabla\cdot\mathbf{v}\mathbf{I}$$

we have the parallel viscosity contribution:

$$\mathbf{t}_{\parallel} = -3\mu_{\parallel}s(\mathbf{bb} - \tfrac{1}{3}\mathbf{I}), \tag{2.9}$$

where

$$s \equiv \mathbf{s}\colon \mathbf{bb} = \mathbf{b}\cdot\nabla(\mathbf{v}\cdot\mathbf{b}) - \mathbf{v}\cdot(\mathbf{b}\cdot\nabla\mathbf{b}) - \tfrac{1}{3}\nabla\cdot\mathbf{v} \tag{2.10}$$

and $\mathbf{I}$ denotes the unit dyadic. The second term in s, proportional to the magnetic field curvature, ensures that the parallel viscosity affects even near-incompressible disturbances ($\nabla\cdot\mathbf{v} \sim 0$) in the neighbourhood of mode rational surfaces (where the first term is small).

3. Equilibrium and Perturbation Equations

The plasma equilibria of interest are specified by $\mathbf{v}_0 \simeq 0$, and prescribed functions that must satisfy the equilibrium field equations,

$$\nabla p_0 = \mu_0^{-1}(\nabla\times\mathbf{B}_0)\times\mathbf{B}_0, \tag{3.1}$$

$$\nabla\cdot\mathbf{B}_0 = 0. \tag{3.2}$$

For a static equilibrium ($\mathbf{v}_0 = 0$), strictly speaking there is also the condition $\nabla \times (\eta \nabla \times \mathbf{B}_0) = 0$ where $\eta = (\mu_0 \sigma)^{-1}$ denotes the zero-order resistivity, but in practice there is a negligible but finite equilibrium resistive diffusion velocity. Nevertheless, this equilibrium velocity is small enough for viscous terms to be omitted from the equilibrium pressure balance equation (3.1), together with inertia.

We denote perturbation quantities by subscript 1, to distinguish them from equilibrium quantities with subscript 0. The linearised first-order visco-resistive equations for small disturbances from a chosen equilibrium are

$$\frac{\partial \rho_1}{\partial t} = -\nabla \cdot (\rho_0 \mathbf{v}_1), \tag{3.3}$$

$$\rho_0 \frac{\partial \mathbf{v}_1}{\partial t} = \mu_0^{-1}[(\nabla \times \mathbf{B}_1) \times \mathbf{B}_0 + (\nabla \times \mathbf{B}_0) \times \mathbf{B}_1] - \nabla p_1 - \nabla \cdot \mathbf{t}_1, \tag{3.4}$$

$$\frac{\partial \mathbf{B}_1}{\partial t} = \nabla \times (\mathbf{v}_1 \times \mathbf{B}_0) - \nabla \times (\eta \nabla \times \mathbf{B}_1), \tag{3.5}$$

$$\frac{\partial p_1}{\partial t} = -\gamma p_0 \nabla \cdot \mathbf{v}_1 - \mathbf{v}_1 \cdot \nabla p_0. \tag{3.6}$$

We are primarily interested in resistive modes driven by magnetic force terms in Eq. (3.4), but no first-order perturbation of the resistivity (leading to rippling instabilities) is included. In this paper, we also omit terms involving the zero-order velocity, which may be important (see, e.g., [10]). These perturbation equations are to be solved subject to appropriate boundary conditions.

4. Viscous Stabilisation

The stabilising nature of magneto-viscosity for ideal or resistive modes can be demonstrated qualitatively as follows. Introducing Lagrangian displacement and magnetic vectors (with reference to the initial position $\mathbf{r}_0$) defined by

$$\frac{\partial \boldsymbol{\xi}}{\partial t} = \mathbf{v}_1(\mathbf{r}_0, t), \qquad \frac{\partial \mathbf{R}}{\partial t} = \mathbf{B}_1(\mathbf{r}_0, t)$$

and integrating with respect to time before eliminating ρ_1 and p_1, we reduce the system of perturbation equations to

$$P\ddot{\underline{\xi}} + K\dot{\underline{\xi}} + D\underline{\xi} = 0. \tag{4.1}$$

Here the dot denotes time derivative, ξ the column six-vector $(\xi, \mathbf{R})^{\mathrm{T}}$, and the coefficient matrices are (cf. also Barston [11]),

$$P=\begin{bmatrix}\rho_0 & 0\\ 0 & 0\end{bmatrix},\qquad K=\begin{bmatrix}L_0 & 0\\ 0 & \mu_0^{-1}L_2\end{bmatrix},\qquad D=\begin{bmatrix}L_1L_3+L_4 & -L_1L_2\\ -\mu_0^{-1}L_2L_3 & \mu_0^{-1}L_2^2\end{bmatrix}$$

with the implicit linear operators

$$\begin{aligned}
&L_0\dot{\xi}=\nabla\cdot\mathbf{t}_1(\dot{\xi}),\\
&L_1\mathbf{R}=\mu_0^{-1}[\mathbf{B}_0\times(\nabla\times\mathbf{R})+\mathbf{R}\times(\nabla\times\mathbf{B}_0)],\\
&L_2\mathbf{R}=\nabla\times(\eta\nabla\times\mathbf{R}),\\
&L_3\xi=\nabla\times(\xi\times\mathbf{B}_0),\\
&L_4\xi=-\nabla(\gamma p_0\nabla\cdot\xi+\xi\cdot\nabla p_0).
\end{aligned}$$

Equation (4.1) is a generalised form for a dissipative system, with magneto-viscosity and resistivity in the dissipative coefficient matrix K, and the resistivity rendering the otherwise ideal MHD coefficient matrix D nondiagonal. For exponential time dependence ($\sim e^{qt}$), from (4.1) we have the quadratic

$$q^2+2\kappa q+\alpha=0 \tag{4.2}$$

with coefficients

$$2\kappa=\int_U \underline{\xi}^*\cdot K\underline{\xi}\,d\tau\Big/\int_U \underline{\xi}^*\cdot P\underline{\xi}\,d\tau,$$

$$\alpha=\int_U \underline{\xi}^*\cdot D\underline{\xi}\,d\tau\Big/\int_U \underline{\xi}^*\cdot P\underline{\xi}\,d\tau,$$

where the asterisk denotes a complex transpose and the integration is taken over the plasma volume U. Thus for $\kappa\geqslant 0$ there is instability if and only if $\mathrm{Re}(\kappa^2-\alpha)^{1/2}>\kappa$, which reduces to $\alpha<0$ for real α when there is no "overstability," i.e., when there is no *oscillatory* growing mode. Equation (4.2) may be compared with the eigenvalue equation for an harmonic oscillator with damping coefficient κ, except that the nett internal force represented by α is not normally restoring. Resistive tearing and magnetic interchange instabilities are driven by terms in the linear operator L_1 contributing to matrix D, and thus to α.

In this paper, we assume that the plasma volume is bounded by a rigid impenetrable perfectly conducting surface S (a *wall*). If $\hat{\mathbf{n}}$ denotes a unit normal on S, the physical boundary conditions at this boundary include vanishing $\hat{\mathbf{n}}\cdot\xi$ (and other components of ξ, in the presence of viscosity), $\hat{\mathbf{n}}\cdot\mathbf{R}$ (or $\mathbf{R}$ on all parts of S at

infinity), and $\hat{\mathbf{n}} \times \mathbf{E}_1$ (so that $\hat{\mathbf{n}} \times (\nabla \times \mathbf{R})$ vanishes). Thus on retaining the dominant parallel viscosity for example, we have the dissipative numerator

$$\int_U \underline{\xi}^* \cdot K\underline{\xi}\, d\tau = \int_U \boldsymbol{\xi}^* \cdot L_0 \boldsymbol{\xi}\, d\tau + \mu_0^{-1} \int_U \mathbf{R}^* \cdot L_2 \mathbf{R}\, d\tau$$

$$= \int_U (3\mu_\parallel |(\mathbf{bb} - \tfrac{1}{3}\mathbf{I}) : \nabla \boldsymbol{\xi}|^2 + \mu_0^{-1} \eta |\nabla \times \mathbf{R}|^2)\, d\tau, \tag{4.3}$$

so that $\kappa > 0$. We expect the parallel viscosity term, supplementing the Ohmic dissipation in (4.3), to be particularly important for large-scale displacements at higher plasma temperatures. We did *not* observe overstability with our computer codes; any unstable mode we found to be purely growing, but damped by parallel ion viscosity (see later). The small growth rate predicted by Eq. (4.2) in the strongly damped limit is $q \simeq |\alpha|/2\kappa$ ($|\alpha| \ll \kappa^2$).

5. Cylindrical Flux Surfaces

Equilibrium cylindrical magnetic flux surfaces, the simplest case of (zero-order) magnetic field curvature, are in general defined by the magnetic field and associated current density of form

$$\mathbf{B}_0(r) = B_{0\theta}(r)\, \mathbf{e}_\theta + B_{0z}(r)\, \mathbf{e}_z, \tag{5.1}$$

$$\mathbf{j}_0(r) = -\mathbf{e}_\theta \mu_0^{-1} \frac{dB_{0z}}{dr} + \mathbf{e}_z (\mu_0 r)^{-1} \frac{d}{dr}(rB_{0\theta}). \tag{5.2}$$

The pressure balance equation (3.1) reduces to

$$\frac{d}{dr}\left(p_0 + \frac{B_0^2}{2\mu_0}\right) = -\frac{B_{0\theta}^2}{\mu_0 r}, \tag{5.3}$$

where the term on the right-hand side arises from field curvature. We consider reverse-field-pinch model equilibria to study wall and magneto-viscous stabilisation of current-carrying plasma.

The force-free Lundquist [12] or "Bessel function model" (BFM) configuration is

$$\mathbf{B}_0(r) = B_0[J_1(\nu r)\, \mathbf{e}_\theta + J_0(\nu r)\, \mathbf{e}_z], \tag{5.4}$$

where J_0 and J_1 are Bessel functions of the first kind, constant B_0 is a measure of the field strength, and ν a measure of the field shear. Another analytic model (FHM) due to Freidberg and Hewett [13] is

$$\mathbf{B}_0(r) = B_0[\tfrac{1}{2}(x - \tfrac{5}{48} a_1 x^3)\, \mathbf{e}_\theta + (1 - \tfrac{1}{12} a_2 x^2)^{1/2}(1 - \tfrac{5}{24} \alpha x^2)\, \mathbf{e}_z] \tag{5.5}$$

so that

$$\frac{dp_0}{dx} = \mu_0^{-1} B_0^2 a_3 \left(x - \frac{5}{6} \alpha x^3 \right). \tag{5.6}$$

Here $x = r/r_p$ with r_p the plasma radius, and constants to satisfy the pressure balance equation (3.1) as functions of the single parameter α are

$$a_1 = \tfrac{1}{3}\alpha(8 - 5\alpha),$$
$$a_2 = \tfrac{1}{9}(8 - 5\alpha)^2,$$
$$a_3 = \tfrac{25}{108}(\alpha - 1)(\alpha - \tfrac{2}{5}).$$

We can set $\alpha = 1$ for a force-free equilibrium ($dp_0/dx = 0$) similar to the BFM, to compare the stability of the two model equilibria. Since the BFM does not include a parallel current gradient driving term, it might be anticipated that the FHM is less stable [5, 13]. The equilibrium profile for the BFM with $\nu = 1$ is shown in Fig. 1a; provided the conducting wall radius $R_w < 5.52$, there is only one field reversal in B_{0z}. For comparison, an equilibrium profile for the FHM (with $\alpha = 1$, $R_w = 3$) is shown in Fig. 1b.

In cylindrical geometry, we assume normal modes of form:

$$f_1(r, t)\, e^{i(m\theta + k_z z)}.$$

Referring to Eqs. (3.3)–(3.6), we find there are six coupled scalar equations to solve in $B_{1r}(r, t)$, $B_{1\theta}(r, t)$, $v_{1r}(r, t)$, $v_{1\theta}(r, t)$, $v_{1z}(r, t)$, and $p_1(r, t)$. (The remaining variables $\rho_1(r, t)$ and $B_{1z}(r, t)$ may subsequently be determined from (3.3) and

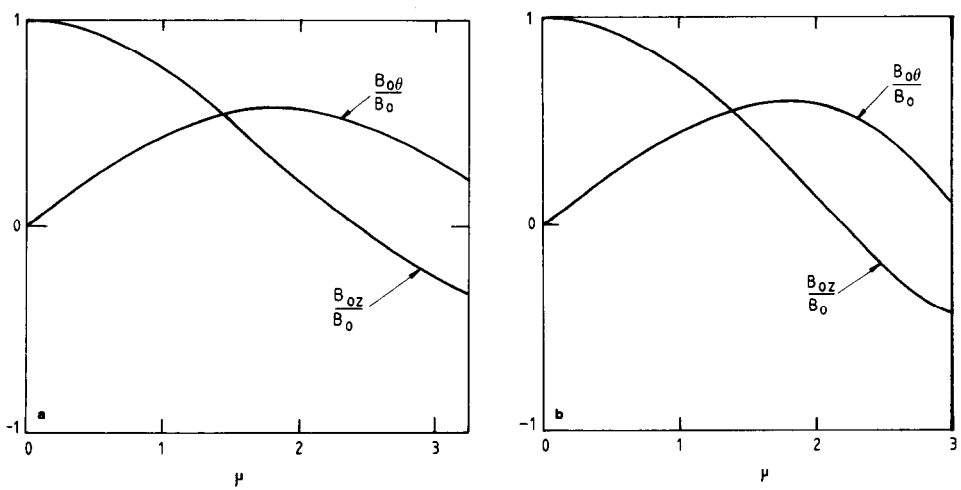

FIG. 1. (a) Bessel function model: equilibrium magnetic fields. (b) Freidberg–Hewett model: equilibrium magnetic fields.

$\nabla \cdot \mathbf{B}_1 = 0$.) We solve these equations on the domain $0 < r \leqslant R_w$, subject to the appropriate conditions.

At $r = 0$ for any time t, there are the symmetry conditions (cf. Dibiase and Killeen [8]):

$$m = 0, \qquad B_{1r} = B_{1\theta} = v_{1r} = v_{1\theta} = 0, \tag{5.7}$$

$$\frac{\partial v_{1z}}{\partial r} = \frac{\partial p_1}{\partial r} = 0,$$

$$m = 1, \qquad \frac{\partial B_{1r}}{\partial r} = \frac{\partial B_{1\theta}}{\partial r} = \frac{\partial v_{1r}}{\partial r} = \frac{\partial v_{1\theta}}{\partial r} = 0, \tag{5.8}$$

$$v_{1z} = p_1 = 0,$$

$$m \geqslant 2, \qquad B_{1r} = B_{1\theta} = v_{1r} = v_{1\theta} = v_{1z} = p_1 = 0. \tag{5.9}$$

At $r = R_w$, for all modes at any time t:

$$B_{1r} = v_{1r} = p_1 = 0, \tag{5.10}$$

$$\frac{\partial}{\partial r}(rB_{1\theta}) = 0, \tag{5.11}$$

$$v_{1\theta} = -iB_{0z}\left(k_z B_{0\theta} - \frac{mB_{0z}}{R_w}\right)^{-1} \frac{\partial v_{1r}}{\partial r}, \tag{5.12}$$

$$v_{1z} = iB_{0\theta}\left(k_z B_{0\theta} - \frac{mB_{0z}}{R_w}\right)^{-1} \frac{\partial v_{1r}}{\partial r}. \tag{5.13}$$

The basic physical conditions for (5.10)–(5.13) are vanishing normal components of perturbed magnetic field and perturbed velocity, and vanishing tangential perturbed electric field, at the rigid perfectly conducting wall. As in earlier work [8], it is also assumed that the perturbed radial current density is negligible near the wall, and the equilibrium pressure p_0 and density ρ_0 tend to zero as $r \to R_w$. We note that the last two conditions (5.12) and (5.13) imply that the perturbed velocity parallel to the (zero-order) equilibrium magnetic field vanishes at the wall, as might be anticipated for a plasma model that incorporates parallel viscosity.

The assumption of negligible perturbed radial current density in the plasma near the wall, previously made in the context of high plasma conductivity [8], may also be viewed as suitable if the plasma has *small* conductivity near the wall (i.e., $\eta(R_w) \to \infty$). One may, for example, consider an insulating liner [13], or that the plasma is otherwise (vacuum) insulated from the wall [14].

To begin the calculation, we assume an initial nonzero perturbation for at least one of the dependent variables, usually $v_{1r}(r, 0)$. The evolution of the dependent variables should ultimately be independent of the initial perturbation, within the

linearisation assumption of the basic perturbation equations (3.3)–(3.6). For the fast growing kink mode $m = 1$, we chose

$$v_{1r}(r, 0) = e^{-c_0}\left[1 - \left(\frac{r}{R_w}\right)^2\right]; \tag{5.14}$$

and otherwise ($m \neq 1$) we chose

$$v_{1r}(r, 0) = e^{-c_0}\left(\frac{r}{R_w}\right)\left[1 - \left(\frac{r}{R_w}\right)^2\right]. \tag{5.15}$$

The parameter c_0 (say 50) is chosen to ensure that the perturbations remain sufficiently small, during the evolution study. These initial perturbation forms were (inter alia) used by Dibiase and Killeen [8]; and we also found that the evolution was ultimately independent of the choice made, but the initial perturbation profiles (5.14) and (5.15) usually provided a smooth development of the dependent variable profiles.

6. Dimensionless Equations: Parallel Viscosity

We follow Dibiase and Killeen [8] by writing the basic plasma equations in dimensionless form, in terms of the following variables:

$$\mu = r/a, \qquad \tau = t/\tau_R,$$

$$\psi = \frac{B_{1r}}{B}, \qquad \phi = i\frac{B_{1\theta}}{B},$$

$$W = -ik\tau_R v_{1r}, \qquad U = k\tau_R v_{1\theta},$$

$$V = k\tau_R v_{1z}, \qquad P = \frac{ip_1}{\langle p \rangle},$$

where a is a characteristic length which is usually a measure of the current layer thickness; $\tau_R = a^2/\langle \eta \rangle$ is the resistive diffusion time; and B, $\langle \eta \rangle$ and $\langle p \rangle$ are characteristic values for the magnetic field, plasma resistivity and pressure, respectively. Resistive instabilities grow on a time scale shorter than the resistive diffusion time τ_R, but longer than the hydromagnetic time $\tau_H = a\sqrt{\mu_0 \langle \rho \rangle}/B$, where $\langle \rho \rangle$ is a characteristic plasma density.

The following dimensionless coupled equations obtained from (3.3)–(3.6) may be used to study the effect of parallel ion viscosity on resistive interchange and tearing modes,

$$\frac{\partial \psi}{\partial \tau} = -FW + \tilde{\eta}\left(L\psi - \frac{2m}{\mu^2}\phi\right), \tag{6.1}$$

$$\frac{\partial\phi}{\partial\tau}=\left(N-\frac{2H}{\mu}\right)\frac{W}{\alpha}-\left(\frac{m}{\mu}H+\kappa_z M\right)\frac{U}{\alpha}$$
$$+\frac{H}{\alpha}\left(\frac{\partial W}{\partial\mu}+\frac{W}{\mu}+\frac{m}{\mu}U+\kappa_z V\right)$$
$$+\tilde{\eta}\left(L\phi-\frac{2m}{\mu^2}\psi\right), \tag{6.2}$$

$$\frac{\kappa_z\tilde{\rho}}{\alpha S^2}\frac{\partial W}{\partial\tau}=\left[\frac{m}{\mu}\left(\kappa_z H-\frac{m}{\mu}M\right)-\frac{M'}{\mu}\right]\psi-M(L\psi)-M'\frac{\partial\psi}{\partial\mu}$$
$$+\left[\frac{m}{\mu}\left(\frac{M}{\mu}-M'\right)+\kappa_z\left(N+\frac{H}{\mu}\right)\right]\phi+\left(\kappa_z H-\frac{m}{\mu}M\right)\frac{\partial\phi}{\partial\mu}+\frac{\beta\kappa_z}{2}\frac{\partial P}{\partial\mu}$$
$$+\frac{\kappa_z\tilde{\rho}\Gamma}{\alpha S^2}\left\{\frac{1}{3}\left(\frac{\partial^2 W}{\partial\mu^2}+\frac{1}{\mu}\frac{\partial W}{\partial\mu}\right)-\left[2f_2f_2'+\frac{3}{\mu}\left(f_2^2-\frac{1}{3}\right)^2\right]\frac{1}{\mu}W\right.$$
$$-\left[\frac{m}{\mu}\left(f_2^2-\frac{1}{3}\right)+\kappa_z f_2 f_3\right]\frac{\partial U}{\partial\mu}-\left[\frac{m}{\mu}f_2f_3+\kappa_z\left(f_3^2-\frac{1}{3}\right)\right]\frac{\partial V}{\partial\mu}$$
$$-\left[\frac{m}{\mu}\left(2f_2f_2'+\frac{3}{\mu}\left(f_2^2-\frac{1}{3}\right)^2\right)+\kappa_z\left(f_2'f_3+f_2f_3'+\frac{3f_2^3f_3}{\mu}\right)\right]U$$
$$\left.-\left[\frac{m}{\mu}\left(f_2'f_3+f_2f_3'+\frac{3f_2f_3}{\mu}\left(f_2^2-\frac{1}{3}\right)\right)+\kappa_z\left(\frac{3f_2^2}{\mu}\left(f_3^2-\frac{1}{3}\right)+2f_3f_3'\right)\right]V\right\}, \tag{6.3}$$

$$\frac{\kappa_z\tilde{\rho}}{\alpha S^2}\frac{\partial U}{\partial\tau}=\left(\frac{m}{\mu^2}M+\kappa_z N\right)\psi+M\left(\frac{m^2}{\mu^2}+\kappa_z^2\right)\phi+\frac{m}{\mu}M\frac{\partial\psi}{\partial\mu}-\frac{\beta\kappa_z m}{2\mu}P$$
$$+\frac{\kappa_z\tilde{\rho}\Gamma}{\alpha S^2}\left[\frac{m}{\mu}\left(f_2^2-\frac{1}{3}\right)+\kappa_z f_2 f_3\right]\left\{\frac{\partial W}{\partial\mu}-3\left(f_2^2-\frac{1}{3}\right)\frac{W}{\mu}\right.$$
$$\left.-3\left[\frac{m}{\mu}\left(f_2^2-\frac{1}{3}\right)+\kappa_z f_2 f_3\right]U-3\left[\frac{m}{\mu}f_2f_3+\kappa_z\left(f_3^2-\frac{1}{3}\right)\right]V\right\}, \tag{6.4}$$

$$\frac{\kappa_z\tilde{\rho}}{\alpha S^2}\frac{\partial V}{\partial\tau}=\left(\kappa_z M'-\frac{m}{\mu^2}H\right)\psi-\frac{m}{\mu}H\frac{\partial\psi}{\partial\mu}-H\left(\frac{m^2}{\mu^2}+\kappa_z^2\right)\phi-\frac{\beta\kappa_z^2}{2}P$$
$$+\frac{\kappa_z\tilde{\rho}\Gamma}{\alpha S^2}\left[\frac{m}{\mu}f_2f_3+\kappa_z\left(f_3^2-\frac{1}{3}\right)\right]\left\{\frac{\partial W}{\partial\mu}-3\left(f_2^2-\frac{1}{3}\right)\frac{W}{\mu}\right.$$
$$\left.-3\left[\frac{m}{\mu}\left(f_2^2-\frac{1}{3}\right)+\kappa_z f_2 f_3\right]U-3\left[\frac{m}{\mu}f_2f_3+\kappa_z\left(f_3^2-\frac{1}{3}\right)\right]V\right\}, \tag{6.5}$$

$$\frac{\partial P}{\partial\tau}=\frac{\gamma\tilde{p}}{\alpha}\left(\frac{\partial W}{\partial\mu}+\frac{W}{\mu}+\frac{m}{\mu}U+\kappa_z V\right)+\frac{\tilde{p}'}{\alpha}W, \tag{6.6}$$

where the operator

$$L \equiv \frac{\partial^2}{\partial \mu^2} + \frac{1}{\mu}\frac{\partial}{\partial \mu} - \left(\frac{m^2+1}{\mu^2} + \kappa_z^2\right).$$

Equations (6.1)–(6.6) involve the dimensionless wavenumber $\alpha = ka$ and axial wavenumber $\kappa_z = k_z a$; the magnetic Reynolds (or Lundquist) number $S = \tau_R/\tau_H$; and the dimensionless viscosity parameter $\Gamma = \tau_R \mu_\parallel / a^2 \langle \rho \rangle$. The equilibrium configuration studied defines the input functions,

$$F = \frac{1}{kB}\left(\frac{m}{r} B_{0\theta} + k_z B_{0z}\right) = \frac{1}{\alpha}\left(\frac{m}{\mu} H + \kappa_z M\right),$$

$$H = \frac{B_{0\theta}}{B}, \qquad M = \frac{B_{0z}}{B}, \qquad N = \frac{1}{\mu}\frac{\partial}{\partial \mu}(\mu H),$$

$$\tilde{\eta} = \frac{\eta_0}{\langle \eta \rangle}, \qquad \tilde{\rho} = \frac{\rho_0}{\langle \rho \rangle}, \qquad \tilde{p} = \frac{p_0}{\langle p \rangle},$$

$$f_2 = B_{0\theta}/\sqrt{B_{0\theta}^2 + B_{0z}^2}, \qquad f_3 = B_{0z}/\sqrt{B_{0\theta}^2 + B_z^2};$$

and the prime denotes differentiation with respect to μ. Equations (6.1)–(6.6) can be solved numerically in $0 < \mu \leqslant \mu_w$ (where $\mu_w = R_w/a$), subject to the dimensionless boundary conditions corresponding to (5.7)–(5.13). These equations could be modified to include other magneto-viscous or nonideal effects. The characteristic plasma parameters adopted were

Resistivity, $$\sigma^{-1} = 1.29 \times 10^4 \frac{\ln \lambda_c}{T^{3/2}}\ \Omega\ \text{cm},$$

Coulomb collision parameter, $$\lambda_c = \begin{cases} 1.239 \times 10^4 \dfrac{T^{3/2}}{n^{1/2}}, & T \leqslant 4.2 \times 10^5\ ^\circ\text{K}, \\ 8.030 \times 10^6 \dfrac{T}{n^{1/2}}, & T > 4.2 \times 10^5\ ^\circ\text{K}, \end{cases}$$

Viscosity (parallel), $$\Gamma = 1.117 \times 10^{-3} \frac{T^4}{n(\ln \lambda_c)^2},$$

Magnetic Reynolds number, $$S = 0.2122 \frac{aBT^{3/2}}{n^{1/2} \ln \lambda_c},$$

Plasma beta, $$\beta = 3.469 \times 10^{-15} \frac{nT}{B^2},$$

Equilibrium density profile, $$\tilde{\rho}(\mu) = 1,$$

Equilibrium resistivity profile, $$\tilde{\eta}(\mu) = 1,$$

in which the physical units adopted are $n = \#/\text{cm}^3$, $T = {}^\circ\text{K}$, $B = \text{G}$, $a = \text{cm}$.

7. VISCODE

A fully implicit finite difference code (VISCODE) of traditional type is described in this section. An implicit scheme is suitable for complicated systems of parabolic or mixed type, on numerical stability grounds [15]. The algorithm for linear tridiagonal systems used by Dibiase and Killeen [8] was implemented for efficiency.

The continuous domain $(0<\mu<\mu_w,\ \tau>0)$ on which the basic perturbation equations (6.1)–(6.6) hold is represented by a discrete space-time mesh,

$$\mu_j = j\Delta\mu, \qquad j=0, 1,..., J,$$
$$\tau^n = n\Delta\tau, \qquad n=0, 1, 2,....$$

The 6 partial differential equations are replaced by a system of $6J$ algebraic (finite difference) equations, which may be solved at successive time-steps (n values) for the dependent variables

$$\psi_j^n = \psi(\mu_j, \tau^n), \qquad \phi_j^n = \phi(\mu_j, \tau^n), \qquad \text{etc.}$$

Space variations are approximated by central differences with implicit weight factor l (for numerical stability, $\frac{1}{2}\leqslant l\leqslant 1$). Thus, if X denotes any dependent variable, space variations are

$$X(\mu, t) = lX_j^{n+1} + (1-l)\, X_j^n,$$
$$LX(\mu, t) = l(LX)_j^{n+1} + (1-l)(LX)_j^n,$$
$$\frac{\partial X}{\partial \mu} = (2\Delta\mu)^{-1}[l(X_{j+1}^{n+1} - X_{j-1}^{n+1}) + (1-l)(X_{j+1}^n - X_{j-1}^n)],$$

where

$$(LX)_j^n = X_{j+1}^n[(\Delta\mu)^{-2} + (2\mu_j\Delta\mu)^{-1}] - X_j^n[2(\Delta\mu)^{-2} + (m^2+1)\,\mu_j^{-2} + \kappa_z^2]$$
$$+ X_{j-1}^n[(\Delta\mu)^{-2} - (2\mu_j\Delta\mu)^{-1}].$$

Time variations are simply

$$\frac{\partial X}{\partial \tau} = (\Delta\tau)^{-1}[X_j^{n+1} - X_j^n].$$

The system of finite difference equations may be written

$$-A_jX_{j+1}^{n+1} + B_jX_j^{n+1} - C_jX_{j-1}^{n+1} = d_j^n, \tag{7.1}$$

where the 6×6 matrices A, B, and C are functions of position (μ_j) only, the input

6-vector d is also a function of the dependent variables X_j^n known at the nth time-step, and

$$X = \begin{bmatrix} \psi \\ \phi \\ W \\ U \\ V \\ P \end{bmatrix}$$

is to be computed at the $(n+1)$th time step for each of the space gridpoints $j = 1,..., J-1$ (given the boundary conditions incorporated at $j = 0$, J, respectively).

The algorithm used to solve the system (7.1) is (cf. [8]),

$$X_j^{n+1} = E_j X_{j+1}^{n+1} + F_j^n, \qquad j = 0, 1,..., J-1,$$

where

$$E_j = (B_j - C_j E_{j-1})^{-1} A_j,$$
$$F_j^n = (B_j - C_j E_{j-1})^{-1} (d_j^n + C_j F_{j-1}^n),$$

for $j = 1, 2,..., J-1$. The boundary conditions at $\mu = 0$, in finite difference form, are used to determine E_0 and F_0^n. The expensive matrix inversion and subsequent generation of E_j is completed before initiating the time-step procedure; which proceeds by a space-sweep forward to calculate F_j^n for $j = 1,..., J-1$ (at successive $n = 0, 1,...$), followed by a backward sweep (with $j = J-1,..., 1$) to calculate X_j^{n+1} for $j = 0,..., J-1$.

8. PDECODE

Any traditional algebraic finite difference code, such as VISCODE, requires a considerable effort to implement. Although special purpose codes may meet special features of a mathematical problem, modern general purpose software can significantly reduce the initial work required and have other advantages [16]. In particular, we are especially interested in future extensions to more sophisticated mathematical models; and prefer to avoid the pre-processing translation (even with the possible help of a symbolic compiler) to finite difference form, implicit in VISCODE alterations.

In this section, we outline the second code (PDECODE) which has been applied in the present context, but may be extended more readily than VISCODE. The development of PDECODE to date required less than 25% of the analytical and programming effort of VISCODE, and has proven to be of comparable efficiency. PDECODE also incorporates user choice of error tolerance with automaic time-

step adjustment, and some user choice of integrator algorithm for the underlying *ordinary* differential equation format produced by the numerical method of lines. For example, since the system of ordinary differential equations produced in our application is typically stiff, the user may choose a suitable integrator algorithm.

PDECODE exploits a general purpose computer software package for numerically solving a system of coupled partial differential equations, called PDECOL [17]. The package PDECOL implements semi-discretization (via the method of lines) with finite element collocation by piecewise polynomials based on *B*-splines for the space dimension, leaving the time dimension for solution by the chosen associated integrator. (PDECOL is a collection of 19 FORTRAN subroutines, so is quite portable.) The user supplied subroutines directly represent the original perturbation equations (6.1)–(6.6), the original boundary conditions (5.7)–(5.13), and the original initial conditions (5.14) and (5.15). No user translation of the basic mathematical problem, for example into finite difference form as in the case of VISCODE, is necessary. We did choose the analytic option for the Jacobian of the system (6.1)–(6.6) however, for computational efficiency. The only significant modification of the package PDECOL we considered was to introduce an alternative Runge–Kutta time integrator STRIDE [18], to improve efficiency with large time-steps for moderate error tolerances compared with the Gear backward difference algorithms (for stiff problems) supplied with the PDECOL package. STRIDE is suitable for stiff problems, and uses a family of singly-implicit Runge–Kutta methods [19] implemented using a transformation given by Butcher [20].

We obtained results from PDECODE, for the mathematical problem defined in Sections 5 and 6, consistent with results obtained from VISCODE. We had anticipated that these codes could be run successfully for low to intermediate values of magnetic Reynolds number S, and in fact found we could obtain results for $S \lesssim 10^5$. Profile broadening when viscosity is included evidently offsets to some extent our present restriction to a fairly course uniform space mesh. We limited our attention to low m modes, primarily $m=0$ and $m=1$. The main difficulty we experienced arose with computations for smaller values of the axial wavenumber k_z.

9. Applications

We chose to test VISCODE and PDECODE with the related BFM and FHM ($\alpha = 1$) equilibria defined in Section 5. The results we obtained for each equilibrium were *qualitatively* similar, as summarised below. We sought to compare our results with corresponding computations by Killeen and others [8, 14]. We also found only purely growing (or decaying) modes with similar time variation and perturbation profiles, although our mathematical model includes parallel viscosity (and the adiabatic assumption), and so is different. For all computations we used the specific heat ratio $\gamma = \frac{5}{3}$, the particle number density $n = 10^{15}\,\mathrm{cm}^{-3}$ and magnetic field strength $B = 1950\,\mathrm{G}$.

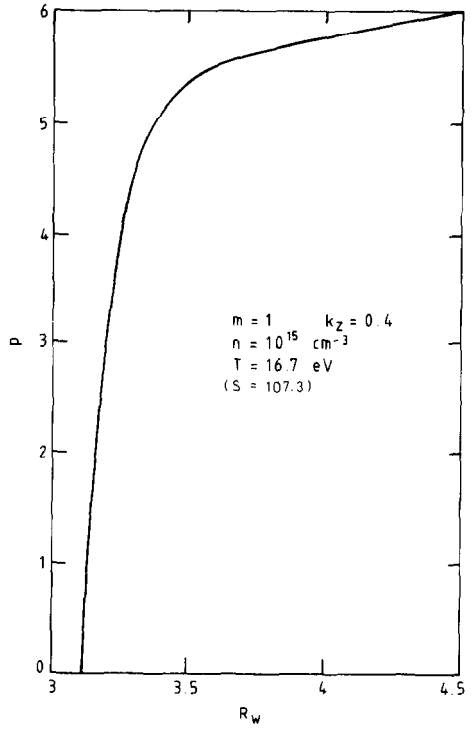

FIG. 2. Bessel function model: growth rate p versus wall position R_W.

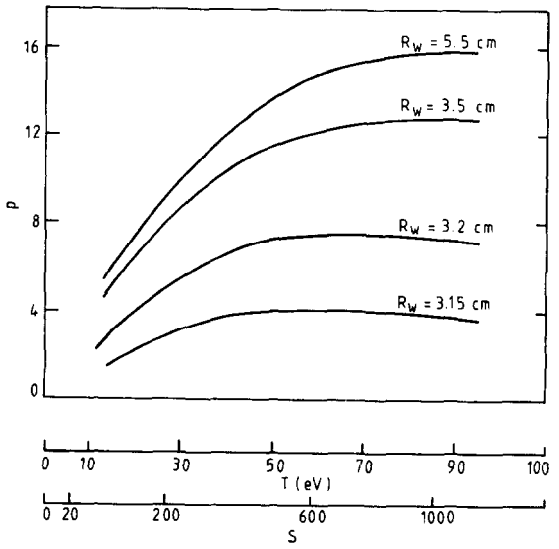

FIG. 3. Bessel function model: growth rate p over a range of temperature T, for various wall radii $m = 1$ visco-resistive kink).

We did find that the fast $m = 1$ kink mode is sensitive to a nearby conducting wall. The sharp cut-off is illustrated in Fig. 2, and the general reduction of growth rate with decreasing wall radius R_w over a range of plasma temperature is shown in Fig. 3, for the BFM (cf. also [8]). However, in addition we found significant stabilisation due to parallel ion viscosity, whatever the position of the conducting wall.

Representative results are shown in Figs. 4a and b, for the BFM and FHM equilibria, respectively. Although the slower $m = 0$ mode is relatively unaffected, the growth rate of the $m = 1$ kink mode can be significantly reduced by parallel ion viscosity. We noted that magneto-viscous stabilisation is most noticeable at shorter wavelengths (i.e., larger wavenumbers k_z) and this is increasingly so as the plasma temperature increases. For the BFM equilibrium, we have chosen to show the somewhat unrealistically large wall radius case ($R_w = 5.5$), partly to allow comparison with the earlier work [8, 14] and partly to gauge the importance of the

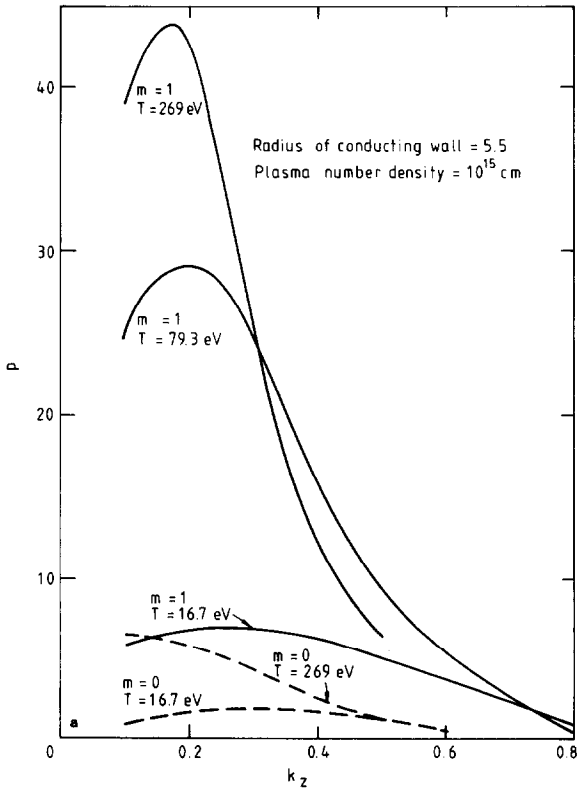

FIG. 4. (a) Bessel function model: growth rate p versus axial wavenumber k_z, for $m = 0, 1$, visco-resistive modes (temperature parameter T). (b) Freidberg–Hewett model: growth rate p versus axial wavenumber k_z, for $m = 1$ visco-resistive kink mode (temperature parameter T).

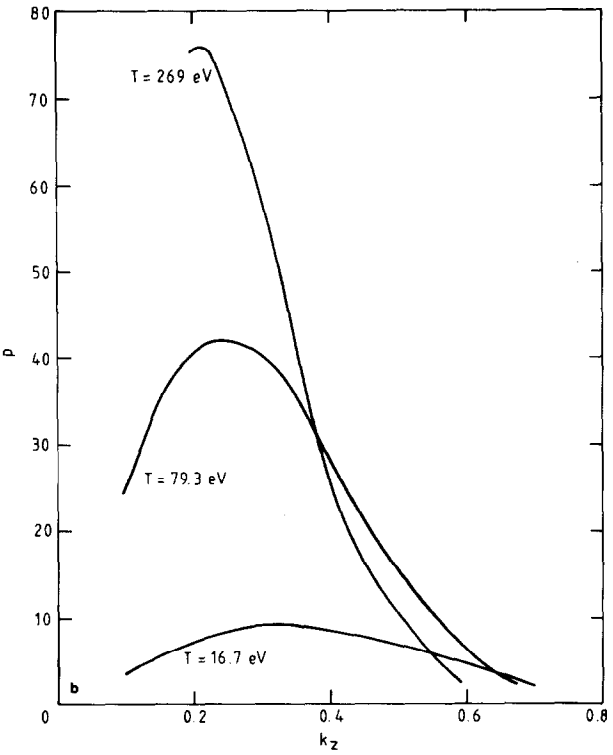

FIG. 4—*Continued.*

parallel current gradient driving term (cf. Sect. 5). Thus the growth rates for the FHM are considerably larger, although the conducting wall radius in this case is much smaller (viz. $R_w = 3$), but the results are qualitatively the same. As in Figs. 2 and 3, the dimensionless growth rate p in Figs. 4a and b is normalised relative to the temperature-dependent resistive diffusion time τ_R [8].

Despite the first impression that may be given by Figs. 4a and b, for the classical transport coefficients adopted (cf. Sect. 6) the magneto-viscous stabilisation becomes significant at all wavelengths, as the plasma temperature increases. Near maximum growth rates in the BFM case of Fig. 4a, renormalised relative to the temperature-independent hydromagnetic time τ_H, are plotted in Fig. 5 on a log–log scale against the magnetic Reynolds number S. We see that the growth rate for the $m = 1$ visco-resistive kink at $k_z = 0.2$, computed from our adiabatic ($\gamma = \frac{5}{3}$) model with parallel ion viscosity, is significantly less than the resistive growth rate at $k_z = 0.3$ found by Shestakov, Killeen, and Schnack [14], for magnetic Reynolds numbers $S \gtrsim 10^4$.

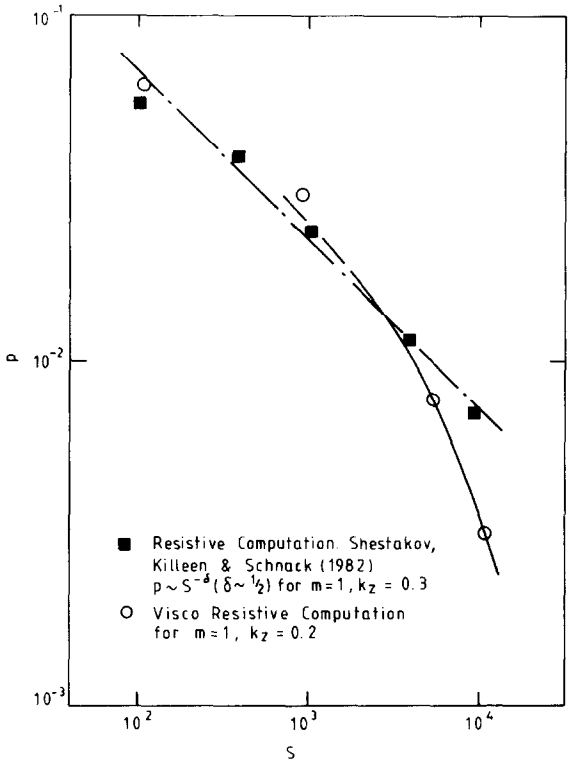

FIG. 5. Bessel function model: near maximum growth rate p (τ_H normalised) versus magnetic Reynolds number S, for $m = 1$ modes. Note that the scales are logarithmic.

ACKNOWLEDGMENTS

It is our pleasure to acknowledge the very helpful advice given by Dr. D. C. Robinson of Culham Laboratory, particularly during the inception of the work described in this paper.

REFERENCES

1. D. C. ROBINSON, *Plasma Phys.* **13**, 439 (1971).
2. H. A. B. BODIN AND A. A. NEWTON, *Nucl. Fusion* **20**, 1255 (1980).
3. M. N. ROSENBLUTH AND M. BUSSAC, *Nucl. Fusion* **19**, 489 (1979).
4. H. P. FURTH, J. KILLEEN, AND M. N. ROSENBLUTH, *Phys. Fluids* **6**, 459 (1963).
5. D. C. ROBINSON, *Nucl. Fusion* **18**, 939 (1978).
6. R. J. HOSKING, *J. Plasma Phys.* **22**, 329 (1979).
7. R. J. HOSKING AND D. C. ROBINSON, in *Ninth European Conference on Controlled Fusion and Plasma Physics* (Oxford, 1979), p. 61.
8. J. A. DIBIASE AND J. KILLEEN, *J. Comput. Phys.* **24**, 158 (1977).
9. R. J. HOSKING AND G. M. MARINOFF, *Plasma Phys.* **15**, 327 (1973).

10. D. DOBROTT, S. C. PRAGER, AND J. B. TAYLOR, *Phys. Fluids* **20**, 1850 (1977).
11. E. M. BARSTON, *J. Fluid Mech.* **42**, 97 (1970).
12. S. LUNDQUIST, *Phys. Rev.* **83**, 307 (1951).
13. J. P. FREIDBERG AND D. W. HEWETT, *J. Plasma Phys.* **26**, 177 (1981).
14. A. I. SHESTAKOV, J. KILLEEN, AND D. D. SCHNACK, *J. Comput. Phys.* **46**, 69 (1982).
15. R. D. RICHTMYER AND K. W. MORTON, *Difference Methods for Initial Value Problems* (Interscience, New York, 1967).
16. M. MACHURA AND A. R. SWEET, *ACM Trans. Math. Software* **6**, 461 (1980).
17. N. K. MADSEN AND R. F. SINCOVEC, *ACM Trans. Math. Software* **5**, 326 (1979).
18. J. C. BUTCHER, K. BURRAGE, AND F. H. CHIPMAN, *BIT* **20**, 326 (1980).
19. K. BURRAGE, *BIT* **18**, 22 (1978).
20. J. C. BUTCHER, *J. Assoc. Comput. Mach.* **26**, 731 (1979).